Elektrotehniški vestnik 76(3): 127–132, 2009
Electrotechnical Review, Ljubljana, Slovenija

fMRI compatible haptic device

Aleš Hribar, Marko Munih

University of Ljubljana, Faculty of Electrical Engineering, Tržaška 25, Ljubljana, Slovenia

Abstract. In this paper an upgrade which enables Phantom haptic device to operate inside fMRI environment is presented. Coupled with a specially designed mechanical extension, Phantom is placed outside strong magnetic field of the fMRI scanner. Mechanical extension enables human subject to manipulate with the Phantom during fMRI scan. Extended haptic system has been subjected to a series of tests to confirm electromagnetic compatibility with an fMRI scanner, for which key results are presented. This fMRI-compatible haptic platform is suitable for studying human brain activation during the execution of preprogrammed virtual environment task. It will allow neuroscientists to study new human motor control functions.

Key words: Phantom haptic device, fMRI, mechanical extension, electromagnetic compatibility, human motor control

fMRI kompatibilni haptični vmesnik

Povzetek. V članku je predstavljena nadgradnja, ki omogoča delovanje komercialnega haptičnega vmesnika Phantom v kliničnem okolju za slikanje z jedrsko magnetno resonanco (fMRI). V ta namen je bil razvit mehanski podaljšek, s katerim je haptični vmesnik odmaknjen na varno razdaljo, stran od visokega magnetnega polja fMRI tomografa. S poizkusi je bilo ugotovljeno, da mehanski podaljšek nima zaznavnega vpliva na haptično percepcijo. Prav tako so poizkusi potrdili elektromagnetno kompatibilnost haptičnega sistema z okoljem magnetne resonance. Predstavljena platforma je primerna za študijo človekovega motoričnega sistema in bo orodje nevrofiziologom za odkrivanje novih procesov v človeških možganih.

Ključne besede: haptični vmesnik Phantom, fMRI, mehanski podaljšek, elektromagnetna združljivost, človeški motorični sistem

1 Introduction

Today, magnetic resonance imaging (MRI) is a standard non-invasive tool used in clinical diagnostics and research into the human body. Over the past few years, a new type of imaging, i.e. the functional MRI (fMRI) has proved to be indispensable in human brain research. The fMRI is based on the measurement of blood oxygen level-dependent (BOLD) signals for estimation of the neural activity in the human brain [1]. In clinical studies [2, 3] researchers have investigated human brain activation during voluntary upper-limb movements. However, a controlled movement task could provide new insights into human motor control. To control and assess the upper limb activity, a device capable of generating and measuring force and trajectories is needed. The device suitable for these and a span of other tasks that depend on position, velocity and acceleration is the haptic robot. To perform haptic movement inside an fMRI scanner, an fMRI-compatible haptic interface is required.

For any device used inside an fMRI environment a high level of safety and electromagnetic compatibility [4] is required. Three major difficulties impose limits on the use of electromechanical devices inside the fMRI scanners. The high magnetic–flux density, which exceeds 1 T in modern fMRI scanners, makes the use of ferromagnetic materials impossible (missile effect). The high–level radio-frequency electromagnetic field and the sensitivity of the scanner receiver coils limit the use of electronic circuits. With a typical diameter of 60 cm, there is also a limited space within the scanner bore. These limitations make the design of an fMRI-compatible device a challenging task.

Several fMRI compatible devices have been developed over the last few years. Chapuis and Gassert [5] and Vogan et al. [6] reported on fMRI-compatible force sensors and actuators. An fMRI-compatible surgical robot with five degrees-of-freedom (DOF) for use inside an intra-operative fMRI scanner was introduced by Chinzei and Miller [7]. The robot is powered by ultrasonic motors.

Research into the field of human motor control requires a tool capable of dynamically controlling arm and hand movements inside an fMRI scanner. A few of such devices have been developed recently. The fMRI-compatible hand rehabilitation devices were introduced by Khanicheh et al. [8, 9]. The 1-DOF haptic interfaces

Received 2 September 2008
Accepted 25 January 2009

were reported [10, 11, 12]. More sophisticated haptic devices have been described [13, 14], one of which has 2-DOF and uses hydraulic actuators to generate force [13]. Another 2-DOF haptic device is powered by an ultrasonic motor[14].

However, to the best of our knowledge, we think that there has been no 3-DOF haptic interface capable of working inside an fMRI environment designed to date. An important issue in the fMRI experiments is the ability to imitate reality inside the scanner as closely as possible. With a three-dimensional haptic-virtual environment reality can be imitated in great detail. This has motivated us to modify the Phantom Premium 1.5 (SensAble Technologies, Inc., Woburn, MA) haptic device to work inside an MRI scanner room. With this widely available and accepted haptic interface we can use all the existing software, thus accelerating design of the system. A mechanical carbon-fiber extension with a 3-DOF joint was developed and coupled to the end-effector of the Phantom haptic device. This ensures that the Phantom can operate at a safe distance, e.g. well outside the high– magnetic field of the main coil of the MRI scanner.

2 Upgrade of the Phantom haptic device

It is a common belief that standard electro-mechanical components have no place inside the fMRI environment as they usually contain some ferromagnetic material. However, in [4] authors defined four zones and showed that it is possible to use some standard components and materials inside the fMRI examination room.

The Phantom Premium 1.5 haptic device is driven by electric coreless motors. For a small electric motor operating inside an fMRI scanner room, the maximum magnetic–flux density permissible is 5 mT [15]. Data supplied by Siemens (Siemens Healthcare, Erlangen, Germany) suggested that the Phantom shall be at a distance of 3 m away from the iso center of the magnet to meet this requirement. The idea was to couple the Phantom with an extension between the end–effector of the Phantom and the subject's hand to satisfy the maximum magnetic–flux density and to allow the subject inside the fMRI scanner to manipulate with the haptic device.

The mechanical extension (Fig. 1) is comprised of two carbon fiber rods, a 2-DOF gimbal, and a linear rail with a carriage. The aluminum part with an $M22\times$ 1.5 thread is glued to the end of each carbon fiber rod. The rods are screwed into a gimbal cylinder, mounted on the main gimbal frame using a bronze axle and Teflon bearings. The main gimbal frame rotates on the bronze shaft mounted on the rail carriage. Stainless steel hex screws are used to secure both axles. The final assembly gives the mechanical extension 3-DOF. The linear rail with the carriage provides a translational DOF and the gimbal adds two rotational DOF.

Figure 1. Exploded view of a 3–DOF joint placed in the middle of the mechanical extension. The joint consists of two rotational DOFs and one linear DOF

The stainless steel rail and RSR9ZM carriage were purchased from THK (THK Company Ltd., Tokyo, Japan). The 2-DOF aluminum gimbal was designed using the Autodesk Inventor (Autodesk, Inc., San Rafael, CA) and manufactured in a CNC machine shop.

At one end, the mechanical extension is coupled with the Phantom haptic device trough a 3-DOF universal joint. The Phantom and the extension are fixed on an aluminium frame assembled from Bosch Rexroth (Bosch Rexroth AG, Lohr, Germany) aluminium strut profiles. Though a wooden frame was planned initially, compatibility tests (described below) demonstrated that it had no notable effect on operation of the fMRI scanner. Another benefit of the aluminum frame is greater mechanical robustness and easy adaptation of the haptic system to different sizes of humans participating in an experiment.

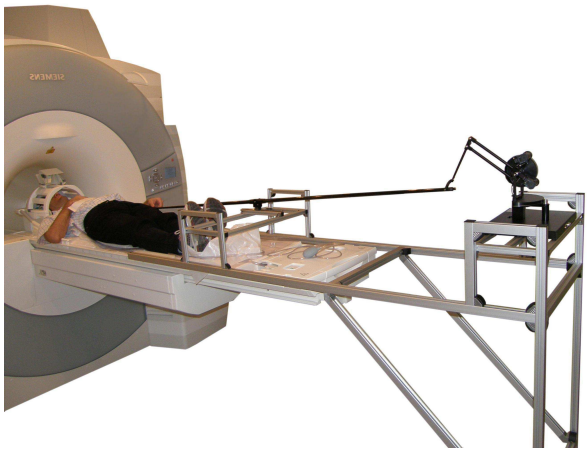

Figure 2. Placement of the extended haptic interface inside the fMRI scanner examination room.

The aluminum frame is bolted together with stainless steel screws. The plastic part connects the sliding examination table of the fMRI scanner and the aluminum frame. The assembly is shown in Fig. 2.

The computer and power amplifier of the Phantom are located outside the fMRI scanner examination room. To minimize electromagnetic interference (EMI), the properly shielded cables, to power and to read the Phantom motors and encoders, are placed as far away from the scanner as possible.

2.1 Kinematics

When the extension is added to the Phantom haptic device, the kinematic map of the haptic system differs from the original Phantom kinematic model derived in [16]. In Fig. 3, a schematic model of the coupled haptic system is shown. The 3-DOF joint of the mechanical extension is described by ϑ_3, ϑ_2 and d_1 variables. The Denavit-Hartenberg parameters of the joint are given in Table 1. These parameters are used to derive forward kinematic matrix $T3$ (Eq. 1):

$$T3 = \begin{bmatrix} -S_3 & -C_3 & 0 & -lS_3 \\ -S_2C_3 & S_2S_3 & -C_2 & -lS_2C_3 \\ C_2C_3 & -C_2S_3 & -S_2 & d_1 + lC_2C_3 \\ 0 & 0 & 0 & 1 \end{bmatrix} \quad (1)$$

in which S_i and C_i denote $\sin(\vartheta_i)$ and $\cos(\vartheta_i)$ where i = 2, 3 and l is the length of the extension.

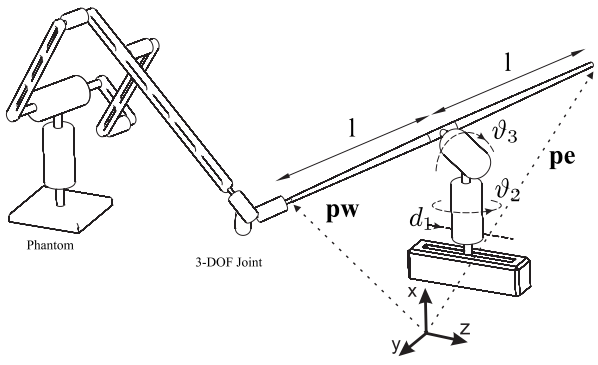

Figure 3. Schematic view of the extended haptic device: the Phantom and mechanical extension.

As we are interested only in the positional part of the transformation first three rows of the last column of the $T3$ matrix are extracted and written as vector **pw** in Eq. 2. The inverse kinematic map of the mechanical extension which is derived from **pw** is represented by Eq. 3. The inverse kinematic equations were solved by using *Wolfram Mathematica® (Wolfram Research, Inc.)*. Results for ϑ_3, ϑ_2 and d_1 are put back into $T3$. The last column of $T3$ matrix represents the kinematic end-to-end solution of the mechanical extension (Eq. 4).

Table 1. DH parameters

Segment	a_i	α_i	d_i	ϑ_i
1	0	$\frac{\pi}{2}$	d_1	$\frac{\pi}{2}$
2	0	$-\frac{\pi}{2}$	0	ϑ_2
3	l	0	0	ϑ_3

$$\mathbf{pw} = \begin{bmatrix} \mathrm{pw}_x \\ \mathrm{pw}_y \\ \mathrm{pw}_z \end{bmatrix} = \begin{bmatrix} -l\sin(\vartheta_3) \\ l\sin(\vartheta_2)\cos(\vartheta_3) \\ d_1 + l\cos(\vartheta_2)\cos(\vartheta_3) \end{bmatrix} \quad (2)$$

$$\mathbf{q} = \begin{bmatrix} d_1 \\ \vartheta_2 \\ \vartheta_3 \end{bmatrix} = \begin{bmatrix} \mathrm{pw}_z + \sqrt{l^2 - {\mathrm{pw}_x}^2 - {\mathrm{pw}_y}^2} \\ -\arccos\left(-\frac{\mathrm{pw}_y}{\sqrt{l^2 - {\mathrm{pw}_x}^2}}\right) \\ -\arccos\left(-\frac{\sqrt{l^2 - {\mathrm{pw}_x}^2}}{l}\right) \end{bmatrix} \quad (3)$$

$$\mathbf{pe} = \begin{bmatrix} \mathrm{pe}_x \\ \mathrm{pe}_y \\ \mathrm{pe}_z \end{bmatrix} = \begin{bmatrix} -\mathrm{pw}_x \\ -\mathrm{pw}_y \\ -\mathrm{pw}_z + 2\sqrt{l^2 - {\mathrm{pw}_x}^2 - {\mathrm{pw}_y}^2} \end{bmatrix} \quad (4)$$

With our software we can read the Phantom end effector trajectories. In order to determine the subject's arm trajectories inside the scanner, we use this kinematic end-to-end solution of the mechanical extension.

2.2 Dynamics

To estimate the impact of the mechanical extension on the subject's performance during execution of the haptic task, a dynamic model of the mechanical extension was designed. For a linear DOF of the joint, the equation can be written as follows:

$$F = m_{ext}\ddot{z} + b\dot{z} \quad (5)$$

and for rotational joints:

$$M = I_{ext}\dot{\omega} + b\omega \quad (6)$$

When moving in a z direction (Fig. 3), an estimation of a force contributed by the extension can be calculated by eq. 5, where F is the force caused by linear DOF, m_{ext} is mass of moving parts of the extension and b is a coefficient of friction. Because the frictional force is small (less than 0.01 N) compared to the force of inertia we can discard the frictional contribution.

For movement in x and y direction a torque contributed by two rotational DOF can be estimated by eq. 6, where M is the torque caused by two rotational DOFs, I_{ext} is matrix of the mass moments of inertia and b is a coefficient of rotational friction. The torque generated by friction in both rotational DOF is in a range of a 10^{-3} Nm therefore it can be discarded.

Additionally static behavior of the extension for x and y direction can be modeled as a spring with a constant k = 140 $\frac{N}{m}$. This way we can describe deflection of the end effector of the extension during static loading.

The mass and mass moments of inertia (I_{ext}) of the mechanical extension were first estimated using the *Autodesk Inventor® (Autodesk, Inc.) physical iProperties* dialog box. The mass value acquired by the *Autodesk Inventor®* was compared with the mass measured by a precision weighting machine. The difference between these two mass values was less than one percent. In all the calculations, the mass value measured with the precision weighting machine is used.

$$m_{ext} = 204 \cdot 10^{-3}\ kg \tag{7}$$

$$I_{ext} = \begin{bmatrix} 3.13 & 0 & 0 \\ 0 & 3.13 & 0 \\ 0 & 0 & 0 \end{bmatrix} \cdot 10^{-2}\ kg\, m^2 \tag{8}$$

By adding mass and increasing the mass moments of inertia of the haptic interface, we expect a slight deterioration of haptic perception. However, for simple haptic tasks to be performed inside the fMRI scanner, we are convinced that the mechanical extension is an effective solution.

3 Test of electromagnetic compatibility

3.1 Test procedure

Experiments described here were carried out to demonstrate electromagnetic compatibility of the extended haptic system with a 3 T Siemens MAGNETOM Trio fMRI scanner of the University Medical Center Ljubljana, Slovenia. The experiments made with the fMRI scanner were accompanied by adequately trained and licensed personnel.

Before the Phantom haptic device was taken inside the fMRI examination room, distribution of the static magnetic field of the scanner had been studied. By using a static magnetic field model supplied by Siemens we determined an approximate position of the Phantom inside the examination room. Future measurements of the magnetic–flux density (usually abbreviated as B) showed that the Phantom would need to be at the distance of 3 m away from the iso-magnetic center of the fMRI scanner to satisfy the maximum allowed flux density in which electric motors of the Phantom may operate.

In the next step, the possible interference of the Phantom operation inside the examination room during fMRI was observed. The tests were carried out on the same day using echo planar imaging (EPI) sequences which are commonly used in brain fMRI examinations. Sequence parameters were fixed throughout experiments (T_R = 3000 ms, T_E = 30 ms, FOV = 192 mm, 36 slices, 6 mm slice thickness, 3x3x3 mm^3 voxel size; T_R – repetition time, T_E – echo time, FOV – field of view). A cylindrical imaging object (plastic bottle 1900 ml, H_2O dist. with solution of: 3.75 g/l $NiSO_4$ x $6H_2O$ + 5 g/l NaCl) was placed inside the scanner. First set of images was acquired without the Phantom inside the examination room. Then the Phantom was placed on the previously determined spot (described above) inside the examination room (Fig. 2). The Phantom was connected to amplifiers, placed outside the room and the virtual environment task was run. The subject inside the examination room was executing the task while another set of images was acquired.

3.2 Test results

The acquired images were analyzed in MATLAB® (The MathWorks, Inc., Natick, MA) as proposed in [17]. The mean pixel value of 30 images of slice 18/36 for both image sets (IMAGE1 and IMAGE2) was first calculated. Then a pixel-by-pixel difference image was acquired using Eq. 9.

$$IMAGE3 = IMAGE1 - IMAGE2 \tag{9}$$

Standard deviation SD of the pixel values within the measurement region of interest (MROI) on IMAGE3 was determined (Eq. 10). The MROI extended over 80 % of the cylindrical imaging object cross-sectional area.

$$SD = \sqrt{\frac{\sum_{i=1}^{n}\sum_{j=1}^{m}(V(i,j) - \overline{V})^2}{2\sum_{i=1}^{n}(m_i - 1)}} \tag{10}$$

In Eq. 10 $V(i,j)$ denotes the pixel value in IMAGE3 and $\overline{V}$ is the average pixel value. The calculated image noise was:

$$IMN = \frac{SD}{\sqrt{2}} \tag{11}$$

The image signal (S) was determined as the mean pixel value within the MROI of IMAGE1. The calculated signal-to-noise ratio (SNR) (Eq. 12) was 172.

$$SNR = \frac{S}{IMN} \tag{12}$$

Figures 4(a)–4(d) present the acquired images during our compatibility experiment. In Fig. 4(a), the mean

value of the first imaging set (30 images of slice 18/36; reference imaging; IMAGE1 in Eq. 9) is shown. Fig. 4(b) shows the mean value of the second imaging set (30 images of slice 18/36; the haptic device running inside examination room; IMAGE2 in Eq. 9). Subtraction of images in Fig. 4(a) and 4(b) is shown in Fig. 4(c) (IMAGE3 in Eq. 9). An inverse of IMAGE3 is presented in Fig. 4(d).

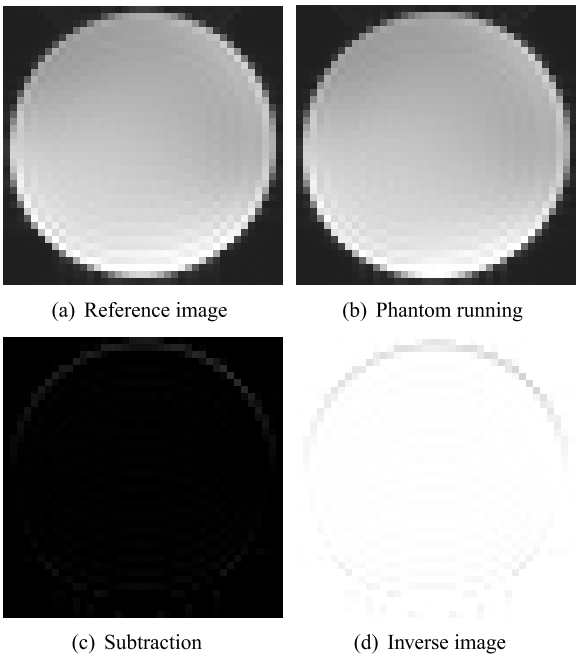

(a) Reference image (b) Phantom running

(c) Subtraction (d) Inverse image

Figure 4. fMRI images of a cylindrical imaging object during the compatibility experiment. Image (a): when no haptic device was present inside the examination room; image (b): when the haptic device was present and running inside examination room; image (c): subtraction of images (a) and (b); image (d): inverse image of the image (c)

In Fig. 4(c), a slight shift of the subtracted images can be observed. This 'ring effect', which can be better seen in Fig. 4(d), was also reported in [7], [9] and [11]. It is not clear whether the shift was caused by haptic device running inside the examination room or by a spatial shift of the imaging object while the two sets of fMRI images were acquired. However, the SNR of images acquired during Phantom operation, is high enough that the we are able to use them to determine regions of the brain activation.

4 Conclusion

The presented upgrade enables the Phantom haptic device to operate inside the fMRI examination room, used together with the fMRI technique, the newly developed tool enables research into human motor control. A comprehensive study demonstrated that it is possible to use it together with the mechanical extension inside the fMRI environment.

Tests confirmed electromagnetic compatibility of the extended haptic device with the Siemens Trio 3T fMRI scanner. Images of the imaging object acquired with the scanner during operation of the haptic device inside the examination room revealed high SNR of 172. The quality of images did not deteriorate while the haptic device was running. With this quality of images, neurophysiologists are able to determine regions of the human brain activation during different controlled motor–oriented upper limb movements.

We believe that the mechanical extension can be used together with other types of the haptic devices (such as the Fokker Haptic Master [18] and MIT Manus [19]) thus enabling them to work inside the fMRI environment. We also suggest that the interaction forces with the haptic environment should be kept within the range of few a Newtons to reduce the human subject head movement during fMRI imaging.

In future, we plan to develop a virtual haptic environment in which human subject will perform different types of motor–orientated tasks. This will allow neurophysiologists to study the human brain activation during controlled upper limb movements.

5 References

[1] S. Ogawa, R. S. Menon, S. G. Kim, K. Ugurbil, "On the characteristics of functional magnetic resonance imaging of the brain", Annu Rev Biophys Biomol Struct 1998; 27: 447–474.

[2] S. Lehericy, E. Bardinet, L. Tremblay, P. F. Van de Moortele, J. B. Pochon, D. Dormont, D. S. Kim, J. Yelnik, K. Ugurbil, "Motor control in basal ganglia circuits using fMRI and brain atlas approaches", Cerebral Cortex 2006; 16: 149–161.

[3] K. Toma, T. Nakai, "Functional MRI in human motor control studies and clinical applications", Magn Reson Med Sci 2002; 1: 109–120.

[4] B. A. Schueler, T. B. Parrish, J. C. Lin, B. E. Hammer, B. J. Pangrle, E. R. Ritenour, J. Kucharczyk, C. L. Truwit, "MRI compatibility and visibility assessment of implantable medical devices", J Magn Reson Imaging 1999; 9: 596-603.

[5] D. Chapuis, R. Gassert, L. Sache, E. Burdet, H. Bleuler, "Design of a simple MRI/fMRI compatible force/torque sensor", In: Proceedings of the 2004 IEEE/RSJ International Conference on Intelligent Robots and Systems; 2004.

[6] J. Vogan, A. Wingert, J. S. Plante, S. Dubowsky, M. Hafez, D. Kacher, F. Jolesz, "Manipulation in MRI devices using electrostrictive polymer actuators with an application to reconfigurable imaging coils", In: Proceedings of the 2004 IEEE International Conference on Robotics and Automation, New Orleans; 2004.

[7] K. Chinzei, K. Miller, "MRI guided surgical robot", In: Proceedings of the 2001 Australian Conference on Robotics and Automation; 2001.

[8] A. Khanicheh, A. Muto, C. Triantafyllou, B. Weinberg, L. Astrakas, A. Tzika, C. Mavroidis, "fMRI-compatible rehabilitation hand device", J NeuroEng Rehab 2006; 3: 24.

[9] A. Khanicheh, D. Mintzopoulos, B. Weinberg, A. Tzika, C. Mavroidis, “MR_CHIROD v.2: A fMRI compatible mechatronic hand rehabilitation device”, In: Proceedings of the 10th IEEE International Conference on Rehabilitation Robotics; 2007.

[10] M. Flueckiger, M. Bullo, D. Chapuis, R. Gassert, Y. Perriard, “fMRI compatible haptic interface actuated with traveling wave ultrasonic motor”, In: Proceedings of the 2005 Industry Applications Conference, 40th IAS Annual Meeting, Vol. 3; 2005: 2075–2082.

[11] N. Yu, W. Murr, A. Blickenstorfer, S. Kollias, R. Riener, “An fMRI compatible haptic interface with pneumatic actuation”, In: Proceedings of the 10th IEEE International Conference on Rehabilitation Robotics; 2007.

[12] R. Gassert, R. Moser, E. Burdet, H. Bleuler, “MRI/fMRI-compatible robotic system with force feedback for interaction with human motion”, IEEE/ASME Trans Mechatronics 2006; 11: 216–224.

[13] R. Gassert, L. Dovat, O. Lambercy, Y. Ruffieux, D. Chapuis, G. Ganesh, E. Burdet, H. Bleuler, “A 2-DOF fMRI compatible haptic interface to investigate the neural control of arm movements”, In: Proceedings of the 2006 IEEE International Conference on Robotics and Automation; 2006.

[14] J. Izawa, T. Shimizu, T. Aodai, T. Kondo, H. Gomi, S. Toyama, K. Ito, “MR compatible manipulandum with ultrasonic motor for fMRI studies”, In: Proceedings of the 2006 IEEE International Conference on Robotics and Automation, Orlando; 2006.

[15] SIEMENS Medical Solutions, MAGNETIC RESONANCE MAGNETOM Trio A Tim System, Technical Drawing, 2006.

[16] M. C. Cavusoglu, D. Feygin, “Kinematics and Dynamics of Phantom model 1.5 Haptic Interface”, Presence: Teleoperators and Virtual Environments 2002; 11(6).

[17] NEMA Standards Publication MS 1-2001, Determination of Signal-to-Noise Ratio (SNR) in Diagnostic Magnetic Resonance Imaging.

[18] W. Harwin and M. Hillman, “Introduction”, Robotica 2003; 21(1): 1–1.

[19] H.I. Krebs, B.T. Volpe, M.L. Aisen, W. Hening, S. Adamovich, H. Poizner, K. Subrahmanyan and N. Hogan, “Robotic applications in neuromotor rehabilitation”, Robotica 2003; 21(1): 3–11.

Aleš Hribar se je leta 2000 vpisal na Fakulteto za elektrotehniko, Univerze v Ljubljani, kjer je dne 11. 09. 2006 diplomiral. Od leta 2006 je mladi raziskovalec v Laboratoriju za Robotiko in Biomedicinsko tehniko na Fakulteti za elektrotehniko, Univerza v Ljubljani. Raziskovalno delo Aleša Hribarja je usmerjeno v načrtovanje, testiranje in uporabo haptičnih robotov v okolju jedrske magnetne resonance oz. funkcionalne jedrske magnetne resonance.

Marko Munih je diplomiral leta 1986, magistriral leta 1989 in doktoriral leta 1993 vse na Fakulteti za elektrotehniko, Univerza v Ljubljani, kjer je sedaj redni professor. Odmevno je raziskoval na University College London. Usmerjenost Laboratorija za biomedicinsko tehniko na Fakulteti za Elektrotehniko je s področja FES privedel na področje rehabilitacijske robotike, oz. haptičnih robotov.